Guided-Mode Resonance and Plasmonic Array Structures for Enhanced Sensing

Introduction

Moxtek has achieved low cost, wafer-scale manufacturing of plasmonic, photonic crystal, and hybrid structures and is ready to support your production needs, from developmental projects through commercialization. Potential applications for these structures include label-free biosensing, surface enhanced Raman spectroscopy (SERS), and microarray-based surface enhanced fluorescence sensing (SEFS). This white paper presents label-free and microarray-based SEFS results for 1-D photonic crystal (PC) sensing utilizing the guided mode resonance (GMR) effect, as well as SERS sensing with 2-D metallic nano-dome arrays utilizing localized plasmonic hotspots.[1]

Experimental results for 1-D photonic crystal guided-mode resonance sensors

The metrology and modeling results depicted in Fig. 1a-1d are for a type of grating-coupled, leaky 1-D photonic crystal (PC) TiO_2 slab waveguide, also called a guided mode resonance (GMR) filter,[2-3] which produces a narrowband reflectance peak that is sensitive to the local refractive index above the grating. Four 1-D PC GMR sensor designs were fabricated with pitch varying from 360 - 410 nm, which allowed for spectral tuning of the resonance for SEFS and label-free sensing applications. Wafer-scale optical metrology tools were used to map out the reflectance uniformity of the GMR sensors using peak wavelength and peak height distributions (Figure 1c) before dicing, though existing tools were found to underestimate the quality of the structures and could not fully resolve the narrower GMR linewidths (<10 nm FWHM). Chip-level measurements of the samples after dicing showed reasonable agreement with modeling and in some cases resonance quality factors (Q) >200 were observed (Fig. 1b), which can be controlled via grating duty cycle (DC), etch depth, and TiO_2 slab waveguide thickness.

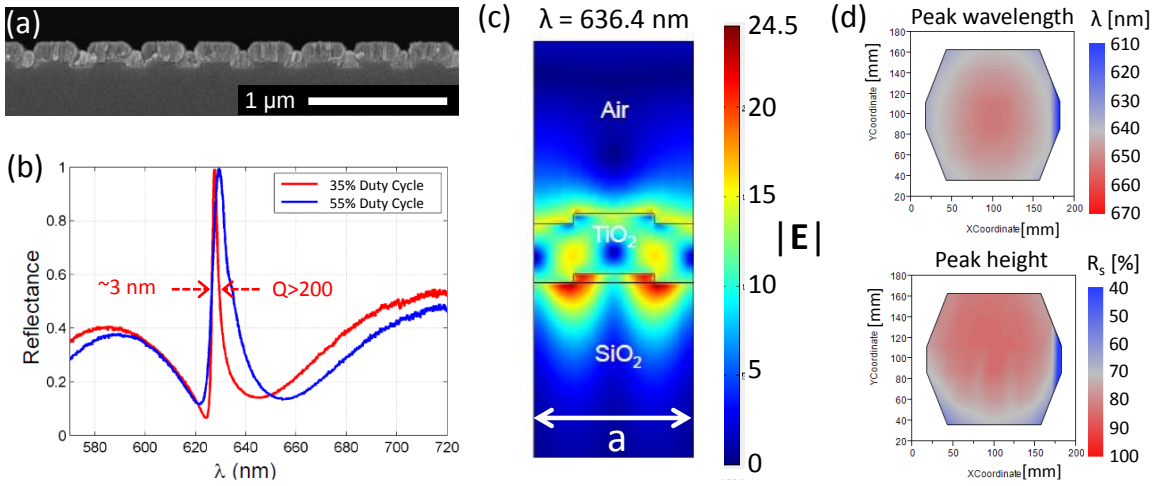

Figure 1. Photonic crystal GMR characterization and modeling results: (a) SEM cross-section, (b) reflectance spectra for gratings with 35% and 55% Duty Cycle, (c) optical model revealing near-field enhancement and field confinement near grating layer, and (d) wafer-level reflectance maps showing uniformity of resonance position and peak height for a 200 mm diameter wafer.

The GMR structures were initially designed for use in an air environment and showed a large shift (~2.5 nm) in resonance position after binding a self-assembled monolayer (SAM) of n-octadecylphosphonate to the TiO_2 waveguiding surface as a way to probe surface-sensing capability (Figure 2a). GMR filters also showed a reasonable shift (~0.3 nm) during *in-situ* label-free sensing in a liquid flow cell configuration (Figure 2b), although some physical (non-covalent) SAM binding may also be taking place on the sample surface. The portion of the resonance shift attributed to covalent SAM formation within the liquid cell was estimated to be ~0.24nm. Spectral sensitivity on the order of 0.03 nm has been demonstrated using a similar GMR filter design on a smartphone-based spectrometer.[4] Hence sub-monolayer detection limits for moderately sized molecules are possible in these GMR sensor systems for label-free detection of surface binding events. These SAM binding studies demonstrate the potential of these GMR filter designs for use as compact label-free sensors, which could be based on either spectral shift in resonance position (as demonstrated), or changes in intensity. Moxtek is now developing PC-GMR designs optimized for in-situ biosensing in aqueous environments. By monitoring the spectral transmittance or reflectance in a properly designed system, these 1-D photonic crystal GMR devices are sensitive enough for applications such as enzyme-linked immunosorbent assays (ELISA) and both DNA and protein microarrays.[4-9]

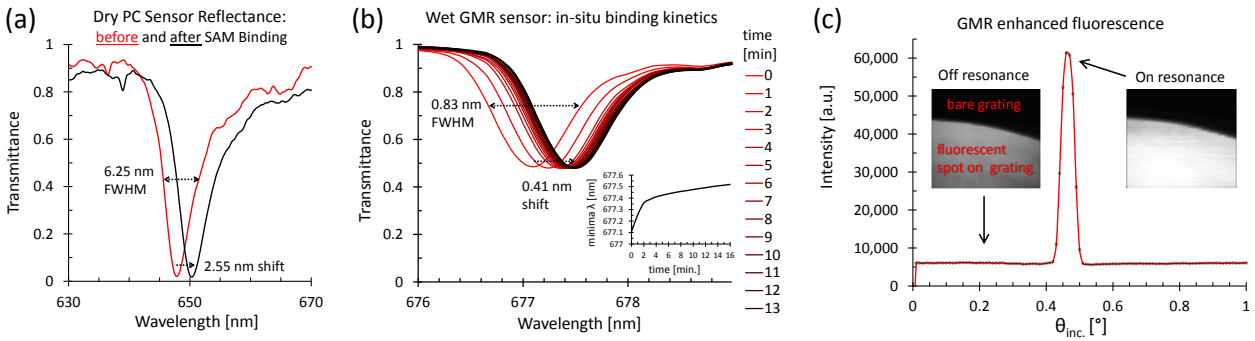

Figure 2. Proof-of-concept for 1-D photonic crystal GMR sensing applications. (a)-(b) Label-free SAM binding studies using transmittance of GMR 1-D photonic crystal structures on fused silica substrates. (a) Dry measurements in air before and after SAM binding procedure. (b) Label-free binding kinetics (inset indicates position of minima vs. time). (c) GMR-enhanced fluorescence intensity vs. excitation angle after spotting. The insets are fluorescence images when the angle is tuned on-resonance and off-resonance, and demonstrate GMR-enhanced fluorescence.

Greater than ten-fold fluorescence intensity enhancement was also demonstrated (Fig. 2c) for a Cy5 dye layer physisorbed to the surface of a filter when the excitation angle was tuned to match the GMR condition, though self-quenching may have limited the overall fluorescence output. The insets depict line-scan fluorescence images taken at the edge of the dye layer at angles of 2.0° (off resonance) and 0.46° (on resonance). The bright regions represent the dye layer, while the dark regions have no dye whatsoever. Larger enhancement factors should be possible with improved laser beam alignment and collimation, and with narrower laser and GMR filter linewidths. In addition, by tuning the 1-D photonic crystal GMR design to enhance both laser excitation and fluorescence emission (utilizing TM *and* TE resonances), 60-328x improvement in fluorescence detection sensitivity and 41-42x increase in signal-to-noise ratio have been demonstrated when compared to a reference slide.[6, 10]

GMR microarrays were then prepared using 1-D PC structures on Silicon substrates, where the resonance position was located near the excitation maxima of Cy5 dye. IgG, IgM, IgA, and Streptavidin-Biotin assays were performed by functionalizing the surface with an epoxy-silane and then covalently grafting the corresponding antigen via spotting at various concentrations followed by standard incubation and washing protocols. The fluorescently labeled antibodies were then introduced at various concentrations using a 16-well array to give a large array of fluorescence spots that were measured using standard fluorescence scanners. The Moxtek GMR substrates showed average enhancements of ~6.7-8.7x in the fluorescence signal minus local background when compared to a bare glass reference slide that underwent the same surface preparation and assay protocols. Similarly, for a bare silicon substrate that underwent the same surface preparation and assay protocols, the Moxtek GMR slides showed ~16.2-27.6x average enhancement. It should be noted that the commercial scanners utilized were not optimized for readout of these photonic crystal structures, which optimally would utilize a well-controlled illumination angle for the exciting source, as demonstrated in Figure 2(c). Current efforts are focused on building such an optimized line-scanning microscope for fluorescence assay readout of these GMR microarray substrates.

Experimental results for 2-D SPR nano-dome array SERS sensors

The 2-D SPR nano-dome array structures depicted in Fig. 3(a)-(b) below utilize a localized surface plasmon hotspot between adjacent domes in order to generate a large field enhancement for SERS applications. They were fabricated using 400 nm pitch SiO_2 posts that were conformally grown with additional SiO_2 before coating with gold. The performance and optical response was most sensitive to the Au layer thickness and Au surface roughness, as well as the separation between reflective Fabry-Perot etalon layers. The gap spacing between adjacent nano-domes was of lesser importance, so long as it remained between 15-30 nm. The reflectance spectra for several experimental designs are given in Fig. 3(c). SERS measurements of Rhodamine 6G dye dried onto sample surfaces are given in Fig. 3(d), which compares background-corrected SERS spectra for a sample coated with rougher gold to that of one coated with smoother gold. The better SERS enhancement was observed for the sample with the smoother gold coatings and with ~25 nm gap spacing, indicating that the nanoscale roughness plays a large part in the Raman enhancement of such structures. The roughened surface likely contributes to the scattering loss of surface plasmons that would otherwise more efficiently couple into the nano-gap. Gold coating thickness and Fabry-Perot etalon spacing was also shown to play an important role in SERS performance (results not shown). Nano-dome arrays with a nano-gap spacing below 15 nm also showed decreased performance.

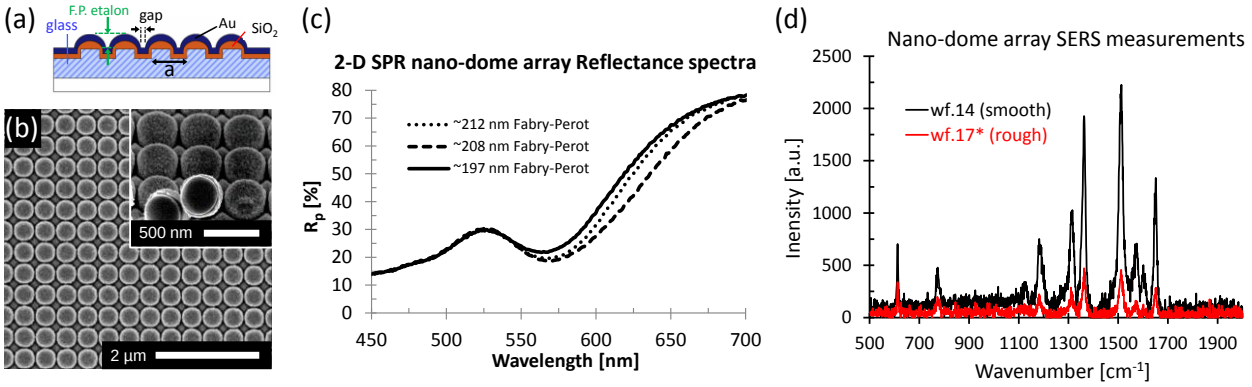

Figure 3. 2-D SPR nano-dome arrays for SERS applications. (a) Schematic cross section. (b) Plan view SEM with perspective view inset of broken sample. (c) Reflectance spectra from wafers with different gold Fabry-Perot etalon layer separations in the normal incidence direction. (d) SERS response for nano-domes with smooth and rough gold coatings.

The SERS response of Rhodamine 6G (R6G) was also measured on a glass reference slide, but no peaks were present, even after increasing both the laser power by a factor of 10 and the concentration by a factor of 1,000. To get a measurable response, the dried R6G spot was positioned such that the laser was instead focused near its edge, where a coffee-ring-like drying effect produced even higher dye concentrations. From this region, weak Raman peaks were visible in the reference sample. The spatially averaged experimental SERS enhancement factor was then calculated as being at least 1.35 x 10^5, based on the ratio of measured Raman intensities at the 1363 cm^{-1} peak (not shown), and corrected by the ratios of laser power and dye concentration for the two samples. This is an underestimate of the true enhancement factor, since the dye was further concentrated by a coffee-ring drying effect in the reference sample. Similar nano-dome array designs have shown 3.16 x 10^6 spatially averaged enhancement factor,[11] with local enhancement factors as large as 1.37 x 10^8. The larger, local enhancement factors are actually normalized by the ratio of the number of molecules within a hot-spot region to the number of molecules within an un-modified laser focal volume. This calculation assumes that most of the SERS signal is coming from a single hot spot between nano-dome arrays and describes only the enhancement that occurs within that region of highest electric field. It doesn't account for the experimental fact that only a portion of the available surface area of the substrate is supporting these hot spots. Hence the spatially averaged enhancement factor, in our case > 1.35 x 10^5, is the experimentally relevant parameter. This result for Au-coated nano-domes is within a factor of 23.4 of previous SERS results on silver-coated nano-dome arrays.[11] Similar nano-dome array designs have been used to demonstrate point-of-care monitoring of intravenous drugs and metabolites, where one could potentially monitor and stop a drug infusion before an unsafe dose reaches a patient, and where clinically relevant detection limits of 20-730 ng/ml were demonstrated.[12-14] Current work is focused on evaluating the gold-coated nano-dome array performance underwater using near-IR excitation, where Au has improved optical properties.

Conclusions

A label-free biosensor designed for use as a microarray substrate showed ~2.5 nm shift in resonance position after monolayer binding. Wafer-scale uniformity maps were prepared and GMR quality factors exceeded 200 for certain designs. Another PC-GMR design was developed for microarray-based SEFS and results from a non-optimized commercial scanner and non-optimized assay protocols produced ~7-28x signal enhancement when compared to reference slides. Furthermore, proper excitation source coupling was shown to produce better than ten-fold enhancement of the fluorescence signal, which should lead to improved assay sensitivity with further substrate and scanner optimization. 2-D nano-dome arrays were also fabricated and showed sensitivity to the gold coating thickness and surface roughness, and to the Fabry-Perot etalon layer separation, while the influence of the gap spacing between adjacent nano-domes was less pronounced. The experimental (spatially averaged) SERS enhancement factor was calculated as being greater than 1.35 x 10^5 for a design with the thinnest gold coating and about 28 nm gap spacing. These high sensitivity, low cost nanostructures are now available on a commercial scale.

Contact Information

Moxtek, Inc.
452 W 1260 N
Orem, UT 84057, USA
www.moxtek.com

Matthew George
Applications Scientist
mgeorge@moxtek.com
+1, (801) 717-4187

References

[1] George, M.C., et al., "Wafer-scale Plasmonic and Photonic Crystal Sensors," Proc. SPIE 9547, Metallic Nanostructures and Their Optical Properties XIII, 95471F (2015). doi:10.1117/12.2188631

[2] Mashev, L., Popov, E., "Zero order anomaly of dielectric coated gratings," Opt. Commun. 55, 377-380 (1985).

[3] Cunningham, B.T., Li, P., Bo, L., Pepper, J., "Colorimetric Resonant Reflection as a Direct Biochemical Assay Technique," Sens. Actuator B 81, 316-328 (2002).

[4] Gallegos, D., et al., "Label-free biodetection using a smartphone," Lab Chip 13, 2124-2132 (2013).

[5] Cunningham, B.T., et al., "Label-Free Assays on the BIND System," Journal of Biomolecular Screening 9, 481-490 (2004)

[6] Block, I.D., et al., "A detection instrument for enhanced fluorescence and label-free imaging on photonic crystal surfaces," Optics Express 17, 13222-13235 (2009).

[7] Choi, C.J., et al., "Comparison of label-free biosensing in microplate, microfluidic, and spot-based affinity capture assays," Analytical Biochemistry 405, 1-10 (2010)

[8] Cunningham, B.T., "Photonic Crystal Surfaces as a General Purpose Platform for Label-Free and Fluorescent Assays," JALA 15, 120-135 (2010).

[9] Long, K.D., Yu, H., Cunningham, B.T., "Smartphone instrument for portable enzyme linked immunosorbent assays," Biomed. Opt. Express 5, 3792-3806 (2014).

[10] Mathias, P.C., Wu, H.-Y., Cunningham, B.T., "Employing two distinct photonic crystal resonances to improve fluorescence enhancement," APL 95, 021111 (2009).

[11] Choi, C.J., et al., "Surface-enhanced Raman nanodomes," Nanotechnology 21, 415301 (2010).

[12] Wu, H.-Y., Cunningham, B.T., "Point-of-care detection and real-time monitoring of intravenously delivered drugs via tubing with an integrated SERS sensor," Nanoscale 6, 5162-5171 (2014).

[13] Wu, H.-Y., Choi, C.J., Cunningham, B.T., "Plasmonic Nanogap-Enhanced Raman Scattering Using a Resonant Nanodome Array," Small 8, 2878-2885 (2012).

[14] Choi, C.J., et al., "Biochemical sensor tubing for point-of-care monitoring of intravenous drugs and metabolites," Lab Chip 12, 574-581 (2012).